EVALUATING THE PERFORMANCE OF AN IMPROVED FINITE VOLUME METHOD FOR SOLVING THE FLUID DYNAMIC EQUATIONS

Frederick Ferguson, Julio Mendez, David Dodoo-Amoo and Mookesh Dhanasar
Mechanical Engineering Department, NCAT, Greensboro, NC 27411, USA

ABSTRACT

One of the most important goals of this research effort is to improve the efficiencies of computational fluid dynamic (CFD) tools by focusing on the development of a numerical procedure with improved flow physics capturing capabilities. The intent is to create a numerical procedure that solves the Navier-Stokes (NS) Equations under a wide variety of initial and boundary conditions, efficiently and accurately. This new scheme, which was initially described in Ref. [1–8] and referred to as the Integro-Differential Scheme (IDS), has several favorable qualities. For instance, the scheme is developed based on a unique combination of the differential and integral forms of the Navier-Stokes Equations, hence the name, IDS. The focus of this paper, however, is on the qualitative evaluation of the IDS solution that were generated from a set of 'commonly described' complex fluid dynamic problems. Among the fluid dynamic problems chosen are (i) the 'inviscid-viscous boundary layer' interaction problem at the leading edge of a hypersonic flat plate, (ii) the 'supersonic rearward facing step' problem, and (iii) the interactions due to the 'sonic jet injection into a supersonic cross-flow'. It is of interest to note, the IDS procedure does not rely on turbulence models, and as such, in analyzing the IDS results of the three selected fluid dynamic problems no such considerations are addressed. Notwithstanding the lack of turbulence models, overall the IDS results compares extremely well with the available experimental data.

INTRODUCTION

The NS equations are a coupled set partial differential equations (PDE) that must be solved with an appropriate set of initial and boundary conditions. These coupled PDEs represent complicated sets of boundary value problems of the type that may manifest themselves in either elliptic, parabolic, hyperbolic or combinations of the aforementioned types. In general, these types of PDEs are complicated and do not lend themselves to analytic solutions. Additionally, aerospace designers are currently demanding improved solutions to fluid dynamic problems under conditions that cannot be duplicated with existing experimental facilities. Hence, the only way to obtain reasonable information on these fluid flow problems lies in the predictions obtained from computational fluid dynamics (CFD) procedures. In the literature, Refs. 9–18, there are many well-established numerical schemes, with many strengths and weaknesses in relations to the current needs of the fluid dynamic community. However, even though, these schemes have led to significant improvements in the art of CFD, they are still fall short in meeting demands posed by the fluid dynamic community. For instance, there are still large efficiencies and expenses when it comes to 'gridding' and 'numerically evaluating' realistic engineering configurations. Besides, there are still great uncertainties when it comes to evaluating the detail physics associated with many 'inviscid-viscous', and 'shock-viscous' interactions. The focus of this paper is on the evaluation of the IDS scheme in relations to its

authors claims of delivering robust, efficient and accurate numerical solutions under a variety of fluid dynamic problems.

THE NAVIER-STOKES EQUATIONS

The equations that govern fluid flows are the continuity, momentum and energy equations. These equations were independently constructed by Navier (1827) and Stokes (1845), and are referred to as the Navier-Stokes equations. In this research, the integral forms of the Navier-Stokes equations, Refs. [9, 12, 13, 19], are of paramount importance. The continuity, momentum and energy equations are listed as follows:

$$\iiint_v \frac{\partial \rho}{\partial t} dv + \iint_s \rho \bar{V} d\bar{s} = 0 \tag{1}$$

$$\frac{\partial}{\partial t} \iiint_v \rho \bar{V} dv + \iint_s \left(\rho \bar{V} . d\bar{s}\right) \bar{V} = -\iint_s P d\bar{s} + \iint \hat{\tau} d\bar{s} \tag{2}$$

$$\frac{\partial}{\partial t} \iiint_v \rho E dv + \iint_s \rho E \bar{V} . d\bar{s} = -\iint_s P \bar{V} . d\bar{s} + \iint_s \hat{\tau} . \bar{V} d\bar{s} + \iint_s \bar{\dot{q}} d\bar{s} \tag{3}$$

In Equations (1) the symbols; ρ, v, t represent the density, the volume of a control fluid element, and time, respectively. In addition, the symbols, $\bar{V}$, $d\bar{s}$ and $\bar{\dot{q}}$, in equations (1–3) represent the vector quantities of the fluid velocity, the control volume surface and the local heat transfer rate. Further, in this research, fluid velocity and the surface element are described through the use of vector quantities as follows:

$$\bar{V} = u\bar{i} + \quad v\bar{j} + \quad w\bar{k} \tag{4}$$

$$d\bar{s} = dydz\,\bar{i} + \quad dxdz\,\bar{j} + \quad dxdy\,\bar{k} \tag{5}$$

$$\bar{\dot{q}} = \dot{q}_x\bar{i} + \dot{q}_y\bar{j} + \dot{q}_z\bar{k} \tag{6}$$

In equations (2) and (3), the symbol, *P*, represents the pressure and the symbol, $\hat{\tau}$, represents a symmetric tensor that defines the various components of the local viscous stresses. This symmetric tensor is described by the equation:

$$\hat{\tau} = \begin{bmatrix} \tau_{xx} & \tau_{xy} & \tau_{xz} \\ \tau_{yx} & \tau_{yy} & \tau_{yz} \\ \tau_{zx} & \tau_{zy} & \tau_{zz} \end{bmatrix} \tag{7}$$

where the symbols of the six independent components, $\tau_{xx}, \tau_{xy}, \tau_{yy}, \tau_{yx}, \tau_{zx}, \tau_{zy}$ and τ_{zz}, are the local shear stress elements that were defined in Ref. [9, 12, 13] as follows:

$$\tau_{xx} = \frac{2}{3}\mu(\nabla . V) + 2\mu\frac{\partial u}{\partial x} \tag{8}$$

$$\tau_{yy} = \frac{2}{3}\mu(\nabla . V) + 2\mu\frac{\partial v}{\partial y} \tag{9}$$

$$\tau_{zz} = \frac{2}{3}\mu(\nabla . V) + 2\mu\frac{\partial w}{\partial z} \tag{10}$$

$$\tau_{xy} = \tau_{yx} = \mu\left(\frac{\partial u}{\partial y} + \frac{\partial v}{\partial x}\right) \tag{11}$$

$$\tau_{xz} = \tau_{zx} = \mu\left(\frac{\partial u}{\partial z} + \frac{\partial w}{\partial x}\right) \tag{12}$$

$$\tau_{yz} = \tau_{zy} = \mu\left(\frac{\partial w}{\partial y} + \frac{\partial v}{\partial z}\right) \tag{13}$$

The symbols, $\dot{q}_x, \dot{q}_y$ and $\dot{q}_z$, in equation (6) represent the components of the heat flux vector in the *x- , y-,* and *z*-directions, respectively. These components are defined by Fourier's law, and expressed mathematically as,

$$\dot{q}_x = -k\frac{\partial T}{\partial x}; \quad \dot{q}_y = -k\frac{\partial T}{\partial y}; \quad \dot{q}_z = -k\frac{\partial T}{\partial z} \tag{14}$$

The symbols, *P* and *E*, in equations (2) and (3) are defined as follows:

$$P = \rho RT; \quad E = C_v T + \frac{u^2 + v^2 + w^2}{2} \tag{15}$$

where R is the gas constant. The symbols, μ, and *k*, represents the viscous and thermal properties of the fluid of interest. In this analysis, the viscosity of the fluid is evaluated through the use of Sutherland's law[9],

$$\mu = \mu_\infty \left(\frac{T}{T_\infty}\right)^{3/2} \frac{T_\infty + 110}{T + 110} \tag{16}$$

In the case of 3D aerodynamic analysis, the Navier-Stokes equations (1)–(16) defined above can be treated as a closed system of five equations relative to five unknowns. These unknowns are the following five primitive flow field variables: $[\rho,\ u,\ v,\ w,\ T]$. It is of interest to note that equations (1 - 16) generates a unique solution set, only when an appropriate set of initial and boundary conditions are provided. Refer to Ref [12, 13] for further details.

THE INTEGRO-DIFFERENTIAL FORMULATION

In the Cartesian Coordinates, a typical fluid flow field is confined to a rectangular block, and represented by a rectangular prism. In the IDS framework, this spatial domain is divided into a collection of elementary cells. Each cell is chosen as infinitesimal rectangular prisms, with unit normal, **ñ**, in the *x, y,* and *z* directions. The dimensions of each cell are defined by *dx, dy*, and *dz,* respectively. Refer to Figure 1. Further, a given cell is defined locally by six independent surfaces, and each surface defined by four points or nodes in a given plane. Additionally, plus and minus notations are used to define the unit normal, **ñ**, with respect to each surface. Next, each surface of each cell is defined by four nodes; namely, nodes-1, nodes-2, nodes-3 and nodes-4. Figure 1b. Illustrates the plus and minus notations for the surfaces with normal to the *z*-direction. It is of interest to note that the use of the object oriented programming concept makes it very convenient to use identical surface objects in the *x* and *y* directions.

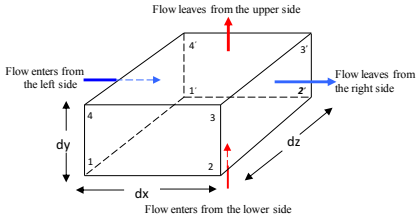

Fig. 1a: Illustration of IDS Spatial Cell

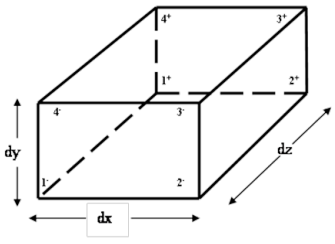

Fig. 1b: Spatial Cell with Notation at Surface Nodes.

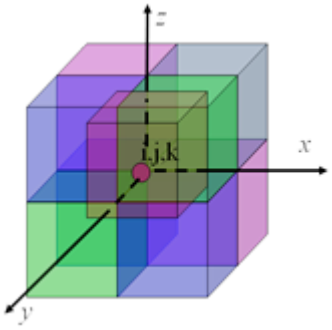

Fig. 2: Illustration of IDS Control Volume

Analogous to 'spatial' cells, the concept of 'temporal' cells is also introduced. The 'temporal' cells are defined as rectangular prisms formed from the center points of eight neighboring 'spatial' cells. Finally, a fluid control volume is defined, as a collection of eight 'spatial' cells and one temporal cell. A typical control volume is illustrated in Figure 2. Each term in the Navier-Stokes equations (1) – (3) are applied systematically to each spatial cell. The mean value theorem is invoked, and a set of algebraic equations representing the rate of change of mass, momentum, and energy associated with each spatial cell is derived. However, the rates of change of the time-fluxes are not associated with any grid point, but with the 'spatial' cell. When the spatial cells are pieced together to form a temporal cell within the control volume, the arithmetic average of the rates of change within the temporal cell then defines rates of change at the *ijk*-point of interest.

Application of the Conservation Laws to the IDS Formulation

To demonstrate the utility of the IDS approach to the conservation laws, consider a typical flow through the surfaces of an infinitesimal control volume, as illustrated in Figure 1. In general, the fluid flows arbitrary in all directions. Even though the *IDS* has the potential to solve 2D as well as 3D fluid-flow problems, for the purpose of simplicity, the discussions conducted in this paper are limited to 2D fluid flow problems. However, when describing the 2D approach, a major challenge involves the conversion of the naturally 3D conservation laws into their 2D counterparts while maintaining the integrity of the 3D flowfield effects. To achieve this outcome, two scientific assumptions are warranted. They are as follows:

1. Using the Cartesian system of coordinates, the control volumes are chosen as infinitesimal rectangular prisms, with unit normal, **ñ**, in the *x, y,* and *z* directions.
2. It was assumed that no flow occurred in the z-direction. In addition, the dimension, dz, of a typical control volume is always a single unit, i.e., dz = 1.

These assumptions led to the fact that the fluid properties in the z-direction across any control volume are constants and the net flow of mass, momentum, and energy in the z-direction is always zero. Consequently, in all surface integration processes, all pertinent terms that are associated with the z-directions as required by the conservation laws are neglected. Armed with these two assumptions, the governing equations are converted into their non-dimensional form and applied on each small control volume. The algebraic form of the rate of change of mass at the center of each cell are evaluated as follow:

$$\left(\frac{\partial \rho}{\partial t}\right)_{Cell,Ctr}^{average} = \left[\frac{\left((\rho u)_1 + (\rho u)_4\right) - \left((\rho u)_2 + (\rho u)_3\right)}{2\Delta x}\right] + \left[\frac{\left((\rho v)_1 + (\rho v)_2\right) - \left((\rho v)_3 + (\rho v)_4\right)}{2\Delta y}\right] \quad (17)$$

In evaluating the momentum and energy equations, careful manipulation of the governing equations necessitates IDS related details in the evaluation of the shear terms. Refer to Ref. [1–8] for greater details.

Explicit Time Marching

In the 2D version of the IDS formulation, the solution vector, $(U_m)_{i,j}^t$, contains the unknown variables, $\rho, u, v,$ and T. Using Taylor's expansion, the solution can be constructed based of the following time marching scheme:

$$(U_m)_{i,j}^{t+\Delta t} = (U_m)_{i,j}^t + \left(\frac{dU_m}{dt}\right)_{i,j} \Delta t \tag{18}$$

where the index ***m*** determine the length of the unknown vector. In the *IDS formulations, the* solution vector, $(U_m)_{i,j}^t$, and its rate of change, $\left(\frac{dU_m}{dt}\right)_{i,j}$, are based on average quantities. However, like all explicit time marching schemes, the time step Δt is subject to a stability criterion. To accurately determine the size of the time step, the following version of the Courant-Friedrichs-Lewy *(CFL*) criterion is used:

$$\left(\Delta t_{CFL}\right) = C\left[\frac{|u_{i,j}|}{\Delta x} + \frac{|v_{i,j}|}{\Delta y} + a_{i,j}\sqrt{\frac{1}{\Delta x^2} + \frac{1}{\Delta y^2}} + \frac{2}{\mathrm{Re}_L}\nu'_{i,j}\left(\frac{1}{\Delta x^2} + \frac{1}{\Delta y^2}\right)\right]^{-1} \tag{19}$$

such that, $a_{i,j}$ is the local speed of sound, $\nu'_{i,j} = \max\left[\frac{4}{3}\mu_{i,j}, \left(\gamma\mu_{i,j}/\mathrm{Pr}\right)\Big/\rho_{i,j}\right]$, *C* is the Courant number, and γ is the specific heat ratio.

EVALUATION OF IDS GENERATED FLOWFIELDS

In efforts to qualitatively verify and validate the capability of the IDS scheme, three established fundamental high Reynolds number fluid dynamics problems were numerically solved and their results carefully analyzed. The problems of interest to this study are as follows: (i) The Inviscid-Viscous interaction problem, (ii) The Supersonic Flow over Rearward-Facing Step Problem, and (iii) The Hypersonic flow cross jet interaction problem**.**

The Hypersonic Inviscid-Viscous Interaction (IVI) Problem

The inviscid-viscous interaction (IVI) problem is defined as the emerging fluid dynamic interactions between an inviscid external flow and the developing boundary layer at the leading edge region of a flat plate Ref, [12, 13, 21]. Many fluid dynamists would agree that this interaction is complex and its prediction requires numerical simulations with very high fidelity Ref. [13, 15, 18, 20, 21]. The flowfield physics of interest to this paper are usually the type of effects that are characterized by high Reynolds numbers. Figure 3 provides a qualitative sketch of the inviscid-viscous interaction phenomenon that is developed as a hypersonic flow traverses a flat plate. Due to the large temperature gradients associated with hypersonic flows, the developing boundary layer is relatively thicker when compared to those at lower speeds. Typically the density within the hypersonic boundary layer is very low as a result of low mass flow rates. Consequently, the streamlines in the boundary layer are displaced outwardly and

the boundary layer thickens. In turn, the approaching hypersonic flow sees a 'blunt body', generates a shock wave which results in higher external pressures. The high external pressure now squeezes the compressible boundary layer and in turn flattens it, thus reducing its strength. The flatten boundary layer with now a weaker shock wave and lower pressure encourages the boundary layer to once again thickens and the interaction cycle continues[21].

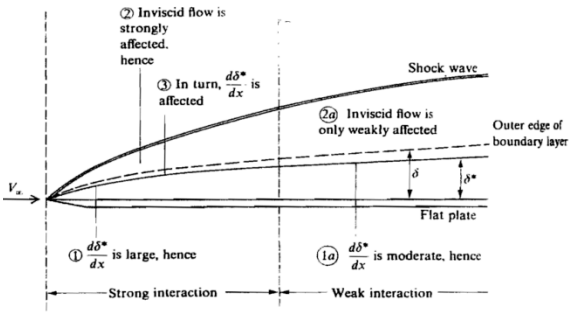

Fig. 3: Illustration of IVI Problem[21]

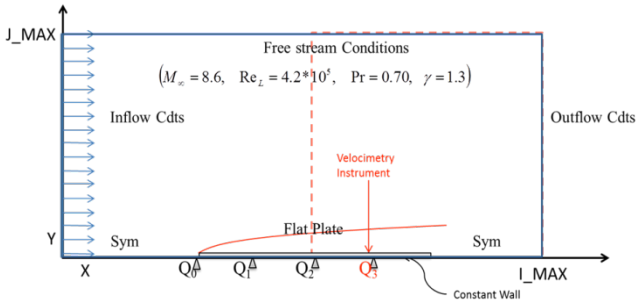

Fig. 4: The IVI Computational Domain

IDS Formulation of the 'Inviscid-Viscous Interaction' Problem

Consider the case of a hypersonic flow over the leading edge of a flat plate at a Mach number of 8.6, Reynolds number of 3.475*10E+6, a Prandtl number of 0.70 and a specific heat ratio, γ, of 1.4. Using the IDS formulation described herein, the 2-D simulation of the resulting hypersonic IVI phenomenon is conducted. The freestream density, temperature, viscosity, and pressure were assumed to be 2.2497*10E-2 kg/m^3, 360K, 2.04E-5 kg/ms, and 2324.39Pa, respectively. Further, the 2D computational domain was developed for a plate length of 1.0 m, and a height of 0.09m. Figure 4 provides a visual representation of the IDS computational domain that encompasses the flat plate. The inflow and outflow conditions are satisfied through the techniques discussed earlier. For the surface boundary conditions no slip at the wall and constant wall temperature were applied.

The 2D IDS formulation provides a set of four independent flowfield parameters that uniquely describes the physics associated with the IVI problem of interest. As part of the IDS evaluation, grid independence studies were conducted at data planes along the leading edge of the plate and at the quarter cord along the plate. The results of these studies are reported in Figures 5a and 5b, and Figures 6a and 6b, respectively.

Analyzing the IDS Predictions of the IVI Phenomenon

The plots illustrated in Figures 5a and 5b show the behavior of the viscous interaction flowfield at the leading edge in the forms of *u* and *v* velocity components. Similar behavior was obtained for the density and the temperature during the IDS grid independence study. In this study, a set of five independent grids with node resolutions in the form: 201 by 201, 401 by 401, 601 by 601, 801 by 801 and 1001 by 1001 were used. A careful observation of the data illustrated in Figures 5a and 5b show that the grid set of 1001 by 1001 delivers a converged solution, and the grid set of 201 by 201 produced the worst resolution.

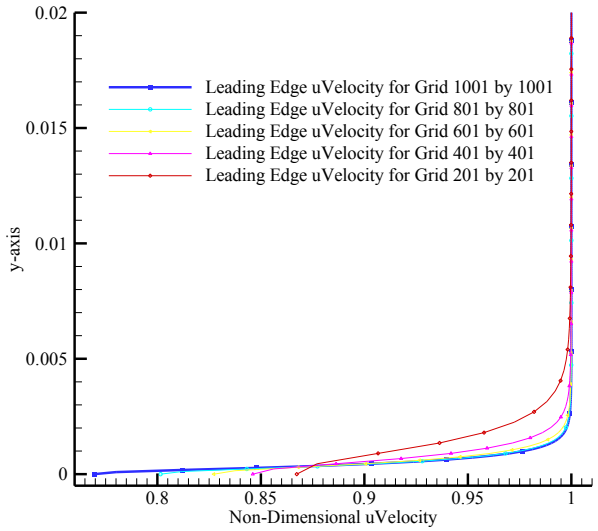

Fig. 5a: uVelocity at Leading Edge

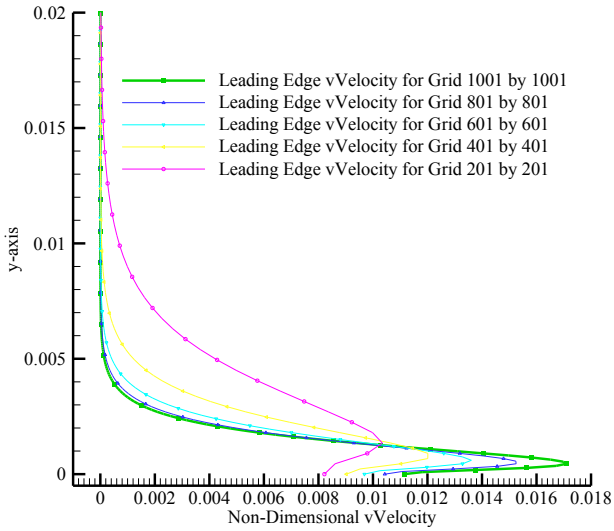

Fig. 5b: vVelocity at Leading Edge

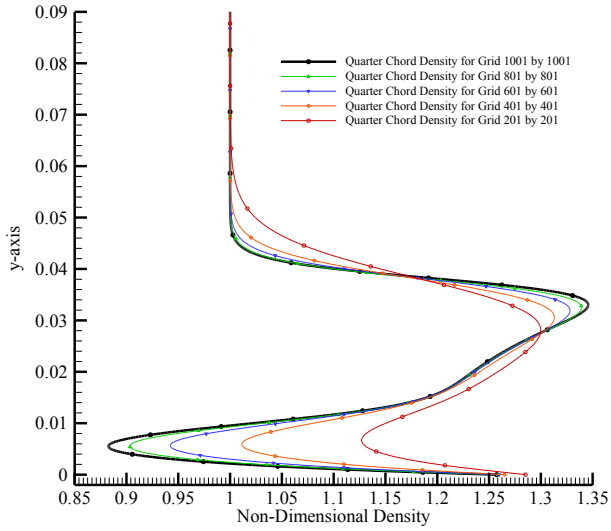

Fig. 6a: Density at Quarter Chord

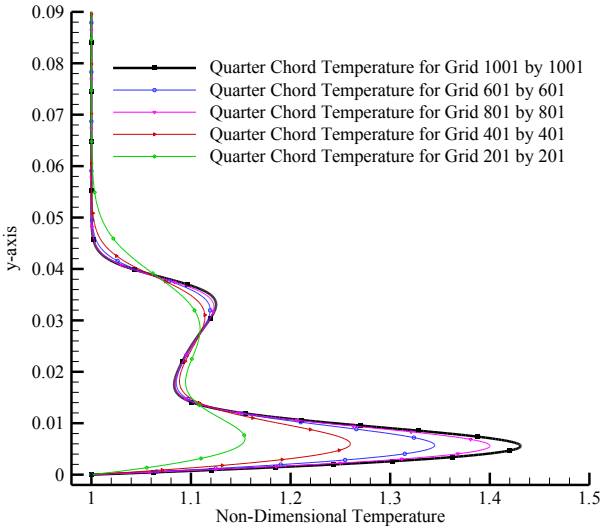

Fig. 6b: Temperature at Quarter Chord

The results of a second set of grid independence study, conducted at the quarter cord of the plate, are plotted and illustrated in Figures 6a and 6b. These plots show the behavior of the IVI flow field in the quarter cord plane along the plate in the forms of *u* and *v* velocity components, density and temperature. Similar to the first study, a set of five independent grids with node resolutions in the form: 201 by 201, 401 by 401, 601 by 601, 801 by 801 and 1001 by 1001 were used. The data sets illustrated in Figures 6a and 6b confirms that the grid set of 1001 by 1001 delivers a converged solution, and the grid set of 201 by 201 produced the worst resolution. In this case, however, it appears that the grids uniformly converge to the best resolution with increasing refinement.

The Supersonic Flow over Rearward-Facing Step Problem

The IDS procedure was used to simulate the supersonic flow over a rearward-facing step (RFS) and its results compared to the experimental analysis conducted by McDaniel et al[22]. Refer to the illustration presented in Figure 7. As seen in Figure 7, several complex flow features, such as, including boundary layer separations and reattachment, and shock wave-boundary layer interactions can be observed Ref. [22–29]. In the supersonic RFS problem, the flow is expected to create an expansion fan as it negotiates the sharp turn and a separation bubble just after the turn. In addition, the bubble and the fan interacts with a free shear layer, which in turns interacts with a developing boundary layer at the base of the step to produce an interesting set of flow field features. As the flow expands and interacts with both the shear layer and boundary layer, a reattachment shock is formed that separates the recirculation bubble from the boundary layer. This reattachment shock forces the flow to become parallel to the walls. It is of interest to note that the flow physics illustrated in Figure 7 was also experimentally observed by a large number of credible researchers Ref. [22–29].

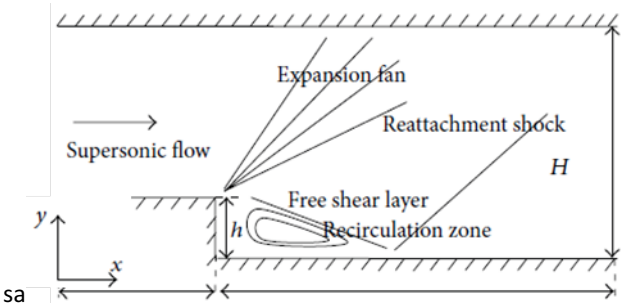

Fig. 7: Supersonic RFS Flow field features

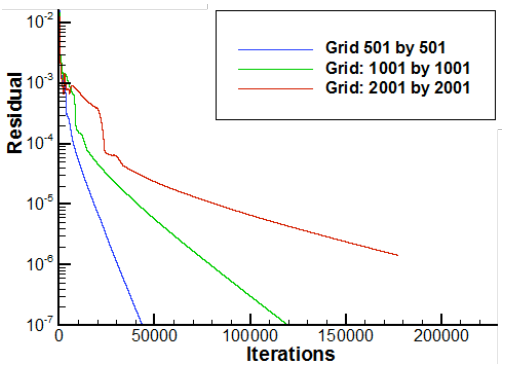

Fig. 8: Grid convergence studies

Rearward Facing Step Grid Convergence Studies

For this IDS investigation, steady state condition was considered to be reached when the maximum residual of the mass, momentum, and the energy fluxes at each internal grid point varied less than 10×10^{-5}. The residual was defined as the difference between the new and the old value of the flux for each two consecutive time steps. The grid convergence study was conducted on three sets of grids; namely, a 501 by 501, a 1001 by 1001 and a 2001 by 2001 grid systems. The residual data obtained from the grid convergence study are illustrated in Figure 8. Figure 8 shows the error decreases with increasing levels of iterations, and that error levels of 10^{-6} and smaller were obtained. During the grid convergence study, the non-dimensional pressure, temperature, and velocity vectors profiles were observed as functions of the non-dimensional height at fixed x-locations. The profile of RFS flow fields parameters at an $x = 5.221H_{step}$ location are presented in Figures 9a and 9b.

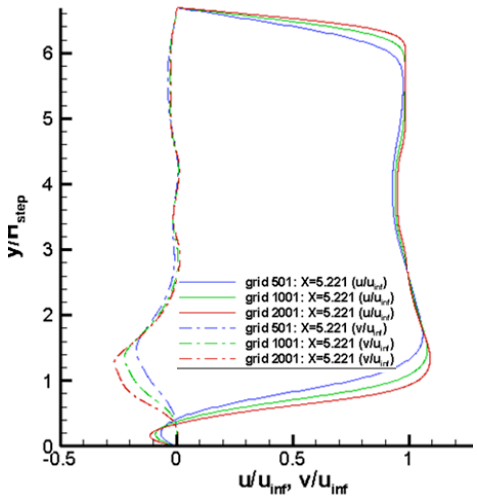

Fig. 9a: Supersonic RFS Flow field features

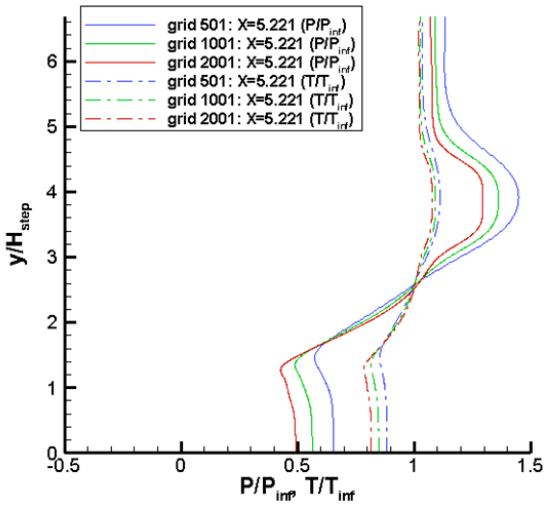

Fig. 9b: Grid convergence studies

Rearward Facing Step IDS-Experimental Comparative Study

For quantitative comparisons of the IDS and experimental data Ref [22], line plots were used. Plots of selected flow field quantities were compared at x-locations: x = $2.465H_{step}$, x = $3.388H_{step}$, x = $5.2208H_{step}$, x = $6.465H_{step}$, x = $10.155H_{step}$. The flow field profiles of non-dimensional pressure, temperature, *u*- and *v*-velocity components are illustrated in Figures 10a and 10b. Figures 10a and 10b illustrate the behavior of the *u*- and *v*-velocity components, respectively. Similar behaviors were obtained for the pressure and the temperature profiles at these locations.

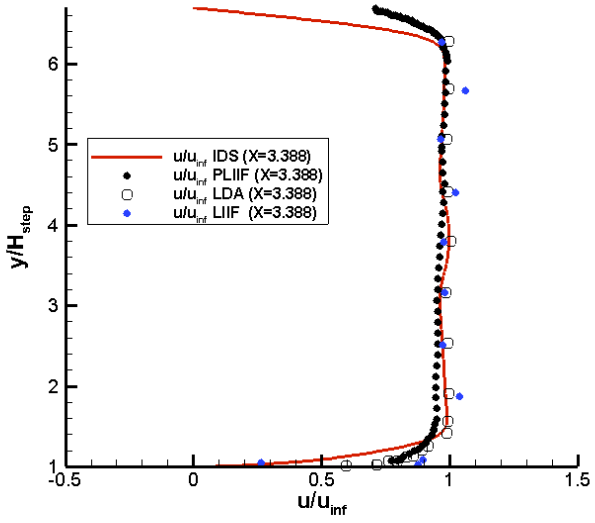

Fig. 10a: Non-dimensional u-velocity Comparisons

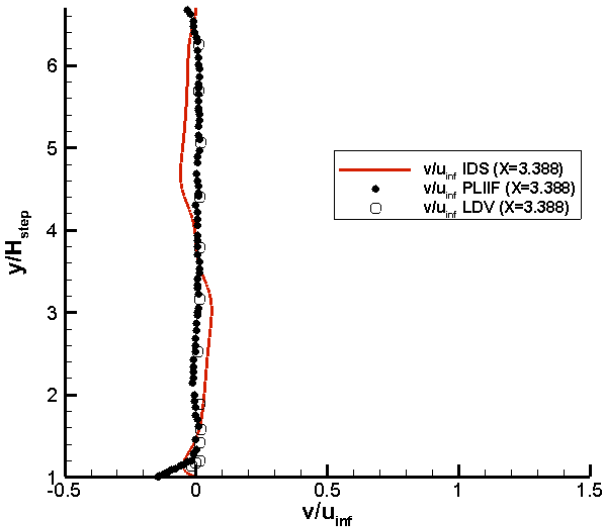

Fig. 10b: Non-dimensional v-velocity Comparisons

As observed, the pressure profile generated by the IDS display higher values when compared to the experiment at the center of the domain. Recall, this discrepancy is due to the leading edge shocks. As the flow moves towards the edge of the RFS, the experimental and numerical

pressure distributions appeared to be very similar. This is due to the fact that the expansion fan is not greatly influenced by the weak leading edge shocks. In the temperature and velocity profiles, the numerical and experimental data are in good agreements. This is expected, since the leading edge shocks and their interactions are very weak and their influence does not affect temperature and velocity profiles. It is noteworthy to point out that the greatest disagreement in the two approaches occurs in the boundary layers and at the walls. In the case of the IDS approach, it is noted that the temperature profile was set to adiabatic, and the actual temperature of the wall was not taken into account.

The Sonic Jet Cross Flow Interaction Problem

The study presented herein focuses on the case of the normal mass injection at sonic speeds through a narrow opening on a plate that is experiencing supersonic flow parallel to its surface. The flowfield boundary conditions of interest to this problem are: (a) the flow travels from left to right, and (b) the freestream conditions are P=1478.26 Pa, T=57.23 K and M=6.0. The main flow features expected from this analysis are schematically shown in Figure 11 Ref [30]. The sonic cross flow interactions are expected to generate the following features: lambda and bow shocks, separation shocks, an incoming thin boundary layer, a distorted barrel shock and the envelope of the jet shear layer, along with regions of separated/recirculation flows. As described in Ref. [30–34], the developing flow field will result in a complex set of aerodynamic flow structures similar to the ones illustrated in Figure 11.

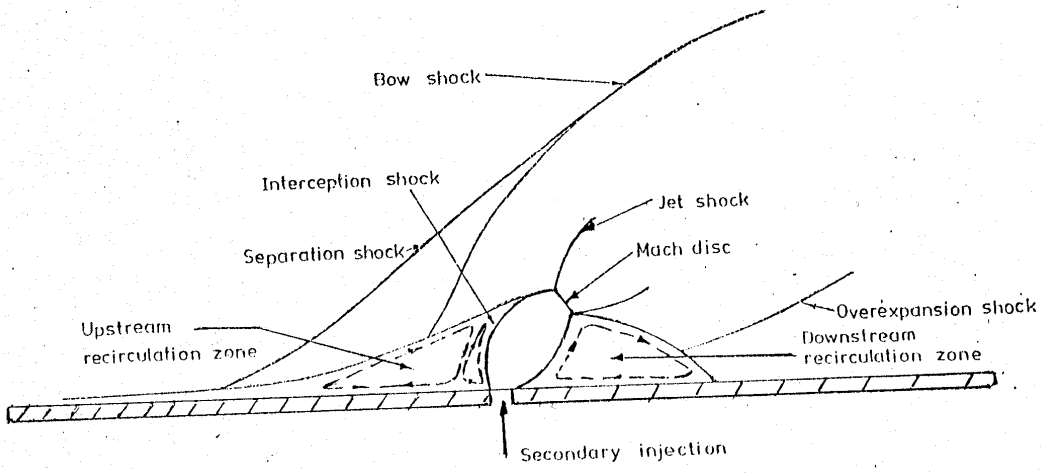

Figure. 11: A Schematic Illustration of the Mach Jet Cross Flow Interaction, Ref. 30

Once again, the IDS formulation is qualitatively evaluated with respect to its capability to reproduce the physics associated with this complex flowfield simulation. Further, the 2D computational domain was developed for a unit non-dimensional plate length and a height of 0.6 m and 0.12 m, respectively. The inflow and outflow conditions were prescribed through the use of the techniques discussed earlier. The surface boundary conditions were set to 'no slip' at the wall, and to adiabatic wall, while the wall density distribution was predicted. The mass flow injection parameters are set as follows: injection speed was set to Mach 1, and the pressure ratio was set to 94.49.

The solution set to the Naver-Stokes equations delivered by the IDS formulation are provided in the four plots illustrated in Figures 12a - 12d. These plots were developed from the four independent flowfield parameters associated with the IDS numerical procedure. In combination, these parameters uniquely describes the physics associated with the problem of interest. In the case of the of the sonic jet interaction problem, the solution are described in Figures 12a – 12d. Figures 12a and 12b illustrate a close-up of the flowfield physics in the region of the emerging sonic jet by highlighting particle stream traces over the contour plots of the *u* and *v* velocity components, respectively. In a similar manner, instead of using the primitive variables, density, the pressure and Mach number distributions are used in Figures 12c and 12d, respectively. In these plots, the pressure and Mach number distributions are used to highlighted flowfield physics in the vicinity of the emerging sonic jet.

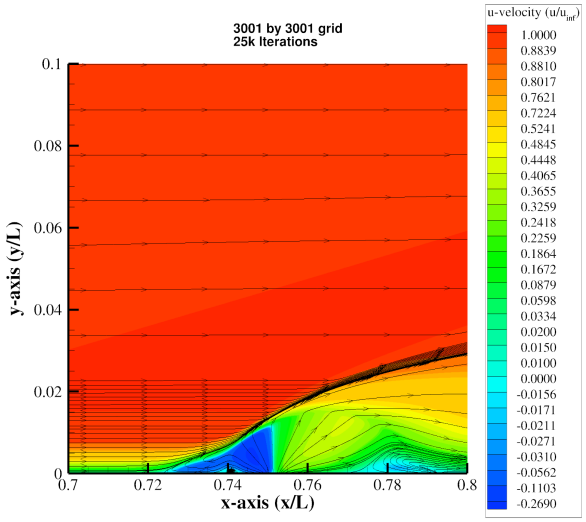

Fig. 12a: Stream traces with u-velocity Contours

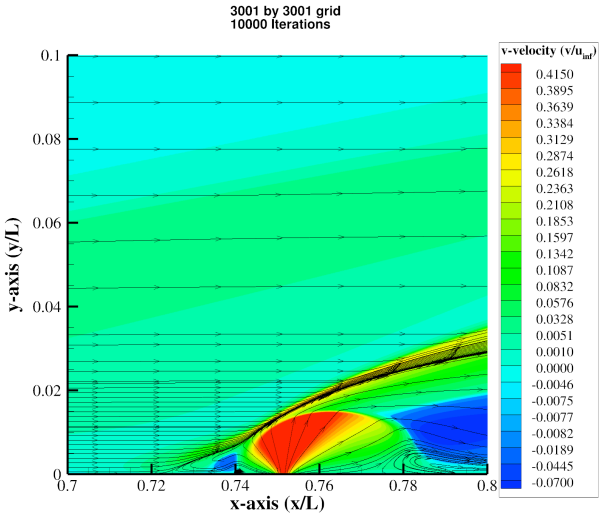

Fig. 12b: Stream traces with v-velocity Contours

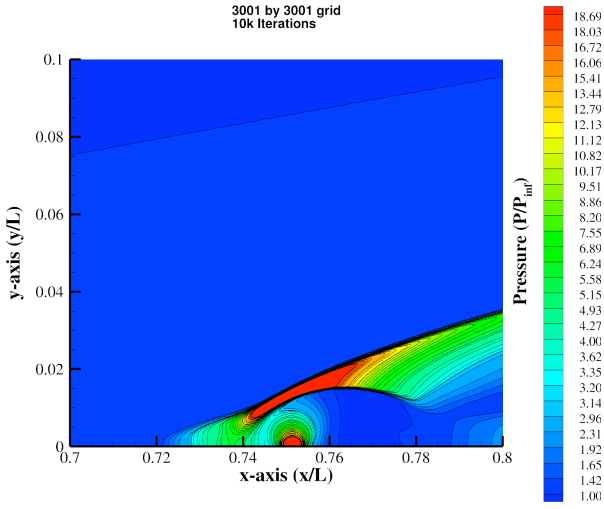

Fig. 12c: Sonic Jet Pressure Contours

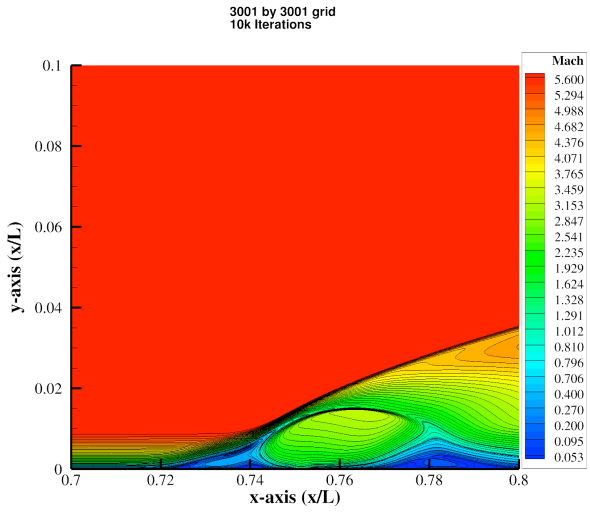

Fig. 12d: Sonic Jet Mach Contours

It can be clearly observed that the details of the flowfield physics, as explained in Figure 11, are captured. Further, it is of interest to note that the details of the many recirculation zones along with the separation and re-attachment points are correctly predicted. On the other hand, Figures 12c and 12d predict the local pressures and Mach numbers distribution in the vicinity of the injection region. Here again it can be observed the recirculation regions, the Mach disk, the local shock waves and expansions fans are all clearly captured. Overall, a careful analysis of the IDS solution for the Sonic Jet Cross Flow problem, showed that the IDS formulation was able to capture the lambda shocks, including the separation and bow shocks. The barrel and recompression shocks , as well as the expansion fan are all clearly predicted. Of greater interest, is the fact that the IDS was able to predict the primary and secondary upstream vortexes, as well as, the primary downstream vortex.

CONCLUSIONS

A numerical procedure for solving the 2D Navier-Stokes equations was developed and validated. This numerical procedure is called the Integro-Differential Scheme (IDS). Its uses a Method of Consistent Averages (MCA) to evaluate the spatial quantities in the flowfield as well as to provide the information need to construct the explicit time marching solution. During the development of the IDS formulation, the concept of a special control volume, consisting of 'spatial' and 'temporal' cells were introduced. The integral form of the Navier-Stokes equations were applied these numerical cell-concepts, and a favorable set of algebraic equations were developed. The numerical procedure resulting from the IDS transformation overcame several limitations of the traditional finite volume schemes.

In this research effort, the IDS numerical procedure was preliminary qualitatively validated through the use of three established boundary layer interaction problems, each with known complexities within its flowfield. Currently, additional efforts are underway to quantitatively validate the IDS code. The results of those studies will be reported at the 2018 AIAA SciTech meetings.

ACKNOWLEDGEMENTS

This work was partially sponsored by the following agencies; AFRL at Eglin Airforce Base, and NASA GRC. In addition, special appreciation is extended to Dr. Isaiah M. Blankson of NASA GRC for his encouragement and support of this project.

REFERENCES

[1] Elamin, Gafar A. (2008). The Integral-Differential Scheme (IDS): A New CFD Solver For The System of The Navier-Stokes Equations With Application. (DOCTOR OF PHILOSOPHY), North Carolina A&T State University.

[2] Elamin, Gafar A. (2004). A CFD Scheme Based on a New and Innovative Method of Consistence Averages. (MASTER OF SCIENCE), North Carolina A&T State University.

[3] Brown, Jovan C. (2011). Validation of the Integral-Differential Scheme as a Navier-Stokes solver via simulation of 2-D Experimental Fluid Studies (Master of Science), North Carolina A&T State University.

[4] Frederick Ferguson, Mookesh Dhanasar , Jovan Brown and Isaiah Blankson. (2012). A Finite Volume Model For Simulating the Unsteady Navier-Stokes Equations Under Space Time Conservations.

[5] Honest F. Mrema (2014), Validation of An Integral-Differential Scheme for Non-Rectangular Domain, (Master of Science), North Carolina A&T State University.

[6] Frederick Ferguson, Honest Mrema, Mookesh Dhanasar, and Isaiah M. Blankson "The Performance Evaluation of an Improved Finite Volume Method for Solving the Navier Stokes Equation" (AIAA Science and Technology Forum and Exposition (SciTech 2015), 5–9 January 2015, Kissimmee, FL); 10.2514/6.2015-0814

[7] Frederick Ferguson, Mookesh Dhanasar, and Nasstaja Dasque, "Validation and Verification of the Navier-Stokes Solutions Obtained from the Applications of the Integro-differential Scheme", 49th AIAA Aerospace Sciences Meeting including the New Horizons Forum and Aerospace Exposition 04–07 January 2011 Orlando, FL; 10.2514/6.2011-1300
[8] Frederick Ferguson, Mookesh Dhanasar, Gafar Elamin, "A Method of Consistent Averages for the Computational Solution to the Fluid Dynamic Equations", ECCOMAS, 5th European Conference on Computational Dynamics, held in Lisbon, Portugal, 14th–17th June 2010.
[9] J. Anderson, G. Degrez, Degroote, E. Dick, R. Grundmann, j. Vierendeels. (2009). Computational Fluid Dynamics-An Introduction (3rd Ed.).
[10] Malalasekera, H. K. Versteeg and W. (2007). An Introduction to Computational Fluid Dynamics: The Finite Voume Method (Second Edition Ed.).
[11] Shang, J. S. (2004). Three decades of accomplishments in computational fluid dynamics. Progress in Aerospace Sciences, 40(3), 173-197. doi: 10.1016/j.paerosci.2004.04.001
[12] Anderson, John D. (1995). Computational Fluid Dynamics: the Basics with Applications.
[13] Chung, T. J. (2002). Computational Fluid Dynamics.
[14] Chakravarthy, S., Goldberg, U., Batten, P., Palaniswamy, S., & Peroomian, O. (2001). Some recent progress in practical computational fluid dynamics. doi: 10.2514/6.2001-136
[15] Oberkampf, William L., & Smith, Barton. (2014). Assessment Criteria for Computational Fluid Dynamics Validation Benchmark Experiments. doi: 10.2514/6.2014-0205
[16] Ijaz, Muhammad. (2010). Computational Fluid Dynamics: A High-Order Temporal Discretization Method
[17] M. Behbahani, M. Hormes, U. Steinseifer, D. Arora, O. Coronado, and M. Pasquali. (2009). A Review of Computational Fluid Dynamics Analysis of Blood Pumps. European Journal of Applied Mathematics
[18] Ebrahimi, Houshang. (2004). An Overview of Computational Fluid Dynamics for Application to Advanced Propulsion Systems. doi: 10.2514/6.2004-2370
[19]P. D., Lax, K., and B., Wendroff, "*Systems of Conservation Laws*", Communications on Pure and Applied Mathematics, Vol. 13, PP. 217-237
[20] Blackaby, N, Cowley, S., Hall, P., On The Instability of Hypersonic Flow Past a Flate, ICASE Report N0. 90-40, NASA Contractor Report 182051, May 1990
[21] Anderson, John D., Hypersonic and High Temperature Gas Dynamics, Second Edition, AIAA Education Series, 2006
[22] McDaniel, James C., Krauss, R. H., Whitehurst, R B., Segal, C., Abbitt III, J D., Experimental Supersonic Hydrogen Combustion Employing Staged Injection Behind a Rearward-Facing Step. (1993) AIAA Journal of Power and Propulsion
[23] Leonard, Rachel and Chokani, Ndaona. (1993). Laser holographic interferometric measurements of the flow behind a rearward facing step. doi: 10.2514/6.1993-3515
[24] Velikorodny, Alexey, Duck, Graham, & Oshkai, Peter. (2010). Experimental investigation of flow over a backward-facing step in proximity to a flexible wall. Experiments in Fluids, 49(1), 167-181. doi: 10.1007/s00348-010-0822-3
[25] D. R. Eklund, D. G. Fletcher, R.J. Hartfield JR. , G. B. Northam, and C. L. Dancey. (1995). A Comparative Computational/Experimental Investigation of Mach 2 Flow Over a Rearward-Facing Step. Computers & Fluids
[26] Liu, Haixu, Wang, Bing, Guo, Yincheng, Zhang, Huiqiang, & Lin, Wenyi. (2013). Effects of Inflow Mach Number and Step Height on Supersonic Flows over a Backward-Facing Step. Advances in Mechanical Engineering, 2013, 1-11. doi: 10.1155/2013/147916 83
[27] Karimi, Abdullah, Wijeyakulasuriya, Sameera, & Nalim, Mohamed. (2012). Numerical Study of Supersonic Flow over Backward-Facing Step for Scramjet Application. doi: 10.2514/6.2012-4001
[28] Yang, A., Hsieh, W., & Kuo, K. (1991). Theoretical study of supersonic flow separation over a rearward facing step. doi: 10.2514/6.1991-2161
[29] Loth, Eric, Kailasanath, K., & Lohner, Rainald. (1990). Supersonic flow over an axisymmetric backward-facing step. doi: 10.2514/6.1990-1580
[30] Isaac, J J., Ramesh, N.R., Sreenath, G.S., Rajashekar, C., Shyamsundar, S.R., Baskaran, M., Venugopalan, P., Gollakota, S., Injection and Peneration of Fuel Jets in Supersonic Crossflows, Dec. 1994, 2nd National Cnoference on Air Breathing Engines and Aerospace Propulsion, VSSC, Thiruvananthapuram

[31]R. S. Amano and D Sun, 'Numerical Simulation of Supersonic Flowfield with Secondary Injection', 24th International Congress of the Aeronautical Sciences, ICAS 2004.
[32] He, H., Yu, J S-T., Three-Dimensional Simulation of Transverse Injection in a Supersonic Flow by the CESE Method
[33] Rama, Z. A., Drikakis, D., Thornber, B.J., Investigation of Sonic Jet Mixing in a Stream of Supersonic Cross-Flow Using Large Eddy Simulations, 27th International Congress of the Aeronautical Sciences
[34] Orth, R.C., Schetz, J.A., Bilig, F.S., The Interaction and Penetration of Gaseous Jets in Supersonic Flow, NASA CR-1386, 1969